This paper describes objective technical results and analysis. Any subjective views or opinions that might be expressed in the paper do not necessarily represent the views of the U.S. Department of Energy or the United States Government.

SAND2021-5732C

LiDAR For Heliostat Optical Error Assessment

Charles Q. Little[1, a)], Daniel E. Small[1, b)], Julius Yellowhair[2, c)]

[1]*Sandia National Laboratories, P.O. Box 5800, Albuquerque, NM 87185 USA.*
[2]*Gryphon Technologies, 2309 Renard Pl SE #120, Albuquerque, NM 87131 USA.*

Corresponding author: [a)] cqlittl@sandia.gov
[b)] desmall@sandia.gov
[c)] jey422@gmail.com

Abstract. This project extends Sandia's experience in **Li**ght **D**etection **A**nd **R**anging (LiDAR) to gain an understanding of the abilities and limits of using 3D laser scanning to capture the relative canting angles between heliostat mirror surfaces in 3D space to an accuracy sufficient to measure canting errors. To the authors' knowledge, this approach has never been developed or implemented for this purpose. The goal is to be able to automatically perform a 3D scan, retrieve the data, and use computational geometry and a-priori mechanical knowledge of the heliostats (facet arrangement and size) to filter and isolate the facets, and fit planar models to the facet surfaces.

FARO FocusS70 laser range scanners are used, which provide a dense data coverage of the scan area in the form of a 3D point-cloud. Each point has the 3D coordinates of the surface position illuminated by the device as it scans the laser beam over an area, both in azimuth and elevation. These scans can contain millions of points in total. The initial plan was to primarily use the back side of the heliostat to capture the mirror (the back side being opaque). It was not expected to capture high-quality data from the reflective front side. The discovery that the front side did, indeed, yield surface data was surprising. This is a function of the soiling, or collected dust, on the mirror surface. Typical point counts on the mirror facets are seen to be between 10k – 100k points per facet, depending on the facet area and the scan point density.

By collecting facet surface points, the data can be used to calculate an individual planar fit per facet, the normals of which correlate directly with the facet pointing angle. Comparisons with neighboring facets yield the canting angles. The process includes software which automatically: 1) controls the LiDAR scanner and downloads the resultant scan data, 2) isolates the heliostat data from the full scan, 3) filters the points associated with each individual facet, and 4) calculates the planar fit and relative canting angles for each facet. The goal of this work has been to develop this system to measure heliostat canting errors to less than 0.25 mrad accuracy, with processing time under 5 minutes per heliostat. A future goal is to place this or a comparable sensor on an autonomous platform, along with the software system, to collect and analyze heliostats in the field for tracking and canting errors in real time. This work complements Sandia's strategic thrust in autonomy for CSP collector systems

INTRODUCTION

Sandia Labs has had a long-standing role in research and development of solar energy systems; in particular, concentrated solar power technology, with heliostats outfitted with multiple facets reflecting sunlight at a target on a central tower. Figure 1 (left) shows the Sandia National Laboratories National Solar Thermal Test Facility (NSTTF) solar tower and heliostat field located in Albuquerque, New Mexico, USA. Figure 1(right) shows a single heliostat in that field. Certainly, the performance of the heliostat field can be impacted by mirror canting errors, tracking errors, and soiling. Each of these issues will reduce the sunlight hitting the target and therefore the performance of the field.

Sandia National Laboratories is a multimission laboratory managed and operated by National Technology & Engineering Solutions of Sandia, LLC, a wholly owned subsidiary of Honeywell International Inc., for the U.S. Department of Energy's National Nuclear Security Administration under contract DE-NA0003525.

FIGURE 1. Sandia NSTTF solar tower and the heliostat field (left) and an NSTTF heliostat with 3D LiDAR Scanner.

Sandia has in the past and continues to develop tools for heliostat focusing and canting enhancement (HFACET) [1 - 2]. In regard to a current project (UFACET) [3], LiDAR scanning was investigated to determine if it could be used to locate the position of a facet in 3D, mostly as a test to acquire truth data. The conventional understanding suggests that LiDAR scanning does not work well on reflective surfaces. Therefore, it was proposed to use checkerboard targets on the corners of the facets. Software would be used to automatically find checkerboard targets, which would provide a simple way to capture the corners of the facet and use those to calculate the plane of the facet. The normal to the plane would render the pointing angle. The position and normal of multiple facets on a heliostat would provide the data to calculate the canting angles. The targets were tested at 10 meters in the lab, and then tested in the field on the heliostat facet corners. The experiment worked better than expected. Figure 2 shows the checkboard target, the resulting LiDAR scan data in the lab at 10 meters, and the resulting LiDAR scan data of the targets placed on the facet corners of a heliostat. To be clear, the scan images in figure 2 are not photographs; they are dense point-clouds that are color-coded from RGB data also taken with the scanner. The points are close enough together to appear as a surface. The black areas in the right image are a tell-tale sign; the image is black where no points were detected.

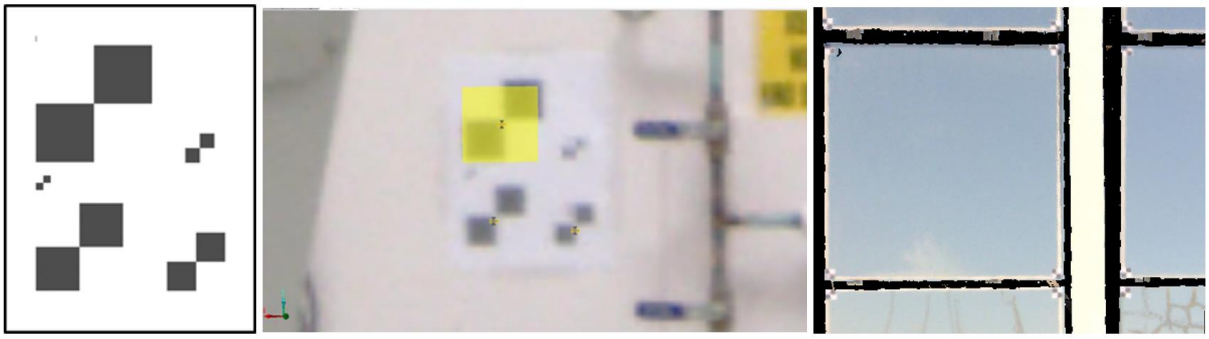

FIGURE 1. Checkerboard; target, scan results on wall at 10 meters, scan result on heliostat facet in field.

As seen in the right image in figure 2, the mirror surface is manifestly visible in the scan data. This was a ‘eureka’ moment. It meant the checkerboard targets are not needed at all. The entire surface of the facet can be used to know its location relative to its neighbors as well as fit a plane to find its pointing angle. The rest of this paper describes how.

LIDAR SCANNING OF HELIOSTATS

A LiDAR scanner uses a laser to detect the distance from the scanner to objects in its surroundings. The technology used is time-of-flight (or phase shift). These scanners typically are mounted on a stationary platform, like a tripod, to maintain a fixed position while scanning. (They can be mounted on moving platforms, but that requires additional localization hardware to combine the data to a single coordinate frame). While the base of the scanner is fixed, the

unit itself uses a rotating mirror to scan vertically and turns the unit to scan horizontally. In this way, data can be captured of an entire area; 360° horizontally and near that (minus the mounting for ~300°) vertically. Range resolution is typically around ± 2 mm. Practical range measurements can be read from ½ m to 50 m or more. The output is a series of locations or points in space. These points come from the reflection of the laser on the surfaces seen by the sensor.

Location here refers to the x-y-z coordinate position of the point relative to the scanner. Most surfaces will adequately reflect laser light, but not all; highly reflective and non-reflective surfaces (coating, black matte) and no surface (open sky and out of range) will have false returns or no return at all. Data consists of values per point: x-y-z position and usually a laser return intensity. In addition, many 3D scanners are co-equipped with visual cameras, and can acquire color (RGB) values for each point. It is not unusual for the output to contain tens to hundreds of million points per scan. Scan times vary with point density, but a typical 50-million-point scan can take less than 5 minutes.

FARO 3D Scanner

For this project, a FARO FocusS70 [4] was used, as shown in figure 3. This unit weighs 10 pounds. With a 45-million-point scan, the corresponding point spacing is 6 mm at 10 m.

FIGURE 2. FARO FocusS70 scanner. (courtesy FARO)

Mirror Surface Results

As mentioned in the introduction it was very surprising to discover that in addition to the checkerboard targets, the mirror surface was also detected by the LiDAR scanner. Figure 4 is an image of the point-cloud data of a heliostat scan. Figure 5 is an RGB image from the same scan. Scanner returns on mirrors with reflections of nearby objects did not return the mirror surface but instead returned the distance to the objects in reflection. This can be seen in the heliostat visible in the reflection in the lower center facets. However, the upper mirror surfaces are present; these have sky reflected in them. Figure 6 shows a closeup of the scan data (this is from a corner where checkerboard targets were placed). Note the density of the data.

FIGURE 3. LiDAR scan of heliostat.

FIGURE 5. Photo of heliostat.

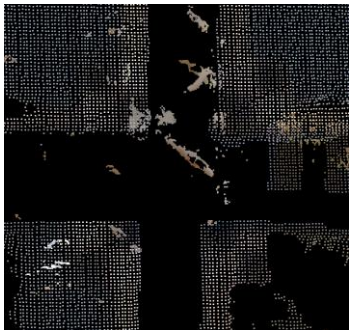

FIGURE 6. Closeup scan data.

Soiled versus Clean Surfaces

It was presumed the scanner was picking up data from the dust or soiling on the mirror surface. The test this theory, half of one of the lower facets of a heliostat was wiped down and scanned. Figure 7 is the result. It is apparent dust makes a difference; it is even obvious the facet was not cleaned very well. Close visual inspection also showed most of the mirrors had a dust layer.

When this proposal was first made, it was based on taking data of a few heliostats at NSTTF, which returned dense point-clouds off the mirror surfaces remarkably well. At the time, it was believed that the normal accumulation of dust on the mirror surface was sufficient to generate good returns. It was not realized how this might be inadequate until the mid-fall of 2019 when NSTTF staff used a common technique to clean all the mirrors simultaneously. This involves waiting for the right kind of weather; a snowstorm of 4 to 6 inches was forecast. As the storm began, the mirrors were oriented to face the sky. After snow accumulated on the horizontal heliostats, they were tilted in elevation to allow the snow to rapidly slide off the mirrors, taking away months of accumulated soiling and dust with it. This resulted in mirrors that were clean across the entire field. Figure 8 shows the results of scanning these clean mirrors. As seen from the images, clean mirrors (seen on the left) do not scan anywhere near as well as soiled ones (seen on the right). The NSTTF heliostat design stows the mirrors upside down, which is believed to be unique in large solar fields. This means that dust will take longer to adhere to the mirror surface.

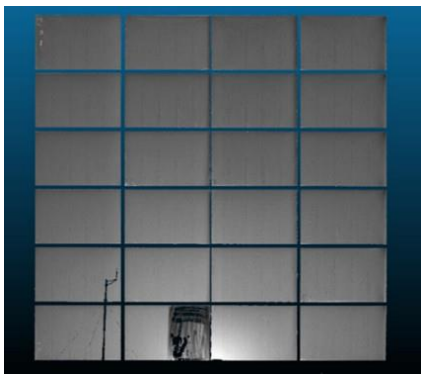

FIGURE 4. Heliostat scan with partially clean facet on bottom row.

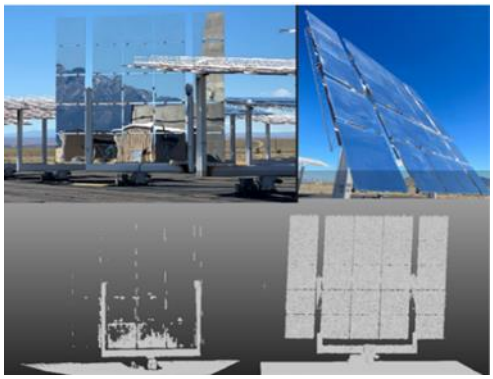

FIGURE 5. Clean vs. Soiled Heliostats.

Since clean mirrors could pose a major limitation to this system, experiments were done with artificially soiling the mirrors by spraying a light cornstarch and water mixture on the heliostat. This artificial soil can be easily washed off. The facets on the right in figure 8 were lightly sprayed with this mixture. Another experiment involved leaving nine of the heliostats facing skyward instead of the ground for a stow position, which allowed them to accumulate dust. Within 5-6 weeks they were able to be scanned without artificial soiling. In a commercial field, the scanning can be performed 180° out of phase from the cleaning cycle which should yield measurable mirror surfaces at most times.

It should be noted that it was not in the scope of this project to quantify the amount of soiling needed for sufficient LiDAR returns.

CANTING ANGLE ESTIMATION

Given that the facet mirror surfaces can be scanned, determining the canting angles of individual facets was the next step. This begins with a full scan of the heliostat, which usually includes the ground around it and other objects in the scan area (see figure 9-A). Each point has an x-y-z value, and the z values can be ordered to estimate and remove the ground (see figure 9-B). The desired heliostat is then isolated from its neighbors or other objects by using connected component analysis (also called blob detection) as shown in figure 9-C. It is assumed the geometry of the heliostat will be known and used as a template to separate the individual facets. The heliostats examined are laid out in a square grid with ample facet separations, so here only the 2D separation distances are being used. This is accomplished by using the major axis of the isolated heliostat and a bounding box algorithm [5] to then translate the data to the X-Y axis. This allows the distance between facet layout of the heliostat to be used to separate each facet. The facet data may yet contain extraneous data. This can be from the support structure that is sometimes scanned through the gaps between facets. An example is shown in figure 9-D.

It is also common for scanning edge effects to give false data. This occurs because the laser beam hitting the edge of objects has a finite dot size, and sometimes partially illuminates more than one surface as it spills over, causing a skirting effect. These bad points can be filtered out. Two methods are used. The first uses the same z ordered filter used for the ground finder; the facet is translated to lie in the x-y plane, and then z ordered, with outliers above and below removed. Figure 9-E shows an example. Another method to filter the facet is to fit a plane and toss points further away from the plane. Both of these methods suppose the vast majority of the points are on the facet. Therefore outliers, which are assumed to be noise or bits of support structure, can be safely removed to enable a better planar estimation of the facet.

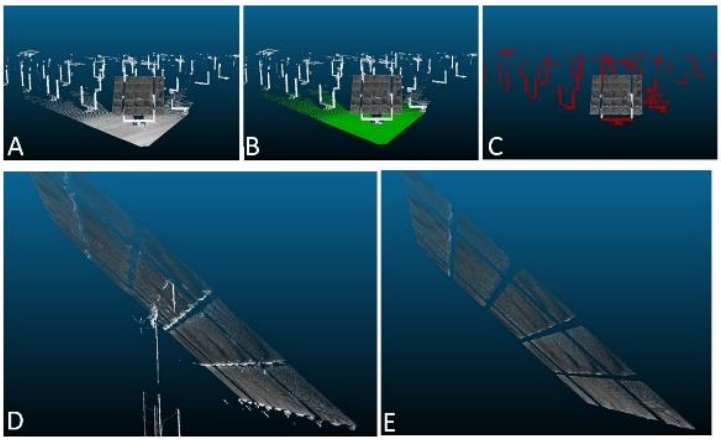

FIGURE 6. A - Full Heliostat Scan, B - Remove the Ground Plane, C - Remove neighboring objects, D - Filter extraneous data on all facets, E - The final filtered facet data.

Finally, with clean facet information, the facet data is fit to planes. This is where the LiDAR scan brings a significant advantage in oversampling, as it can capture upwards of 100,000 points per facet. Because the +/-2 mm range error is zero-mean, the planar estimate error is reduced by $\frac{1}{\sqrt{(N)}}$ (N = total number of points in the facet).

It is known that these facets are not, in fact, planar, but rather parabolic. The planar assumption was made for several reasons. First it is assumed the facets are symmetrical, with the center of the parabola in the center of the facet. This means that the normal will be the same for a parabola or a plane pointing in the same direction. Second, it is much easier to fit a plane than a parabola, especially considering the shallowness of the curvature compared to the resolution limits of the scanner. The assumption was made that the result (canting angle) would be equivalent.

The process subtracts the centroid of each facet data (i.e. translating the facet points to center at the origin) and uses the Singular Value Decomposition method to determine the planar normal, which is used as the facet direction vector. The canting angle must be relative to something, and the center facet is picked as the control vector. Each facet normal is compared to the center facet normal. Figure 10 shows the segmented facets color coded. Figure 11 shows these vectors displayed from the heliostat scan, with the vector originating at the centroid of the facets. Canting angles are reported as azimuth and elevation of each plane relative to the center facet.

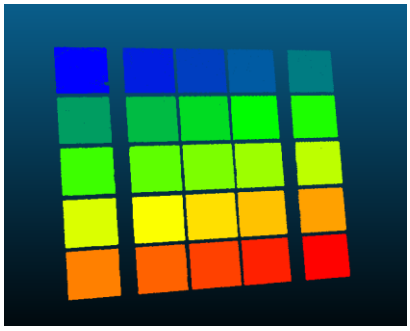

FIGURE 7. Automatically segmented facet data.

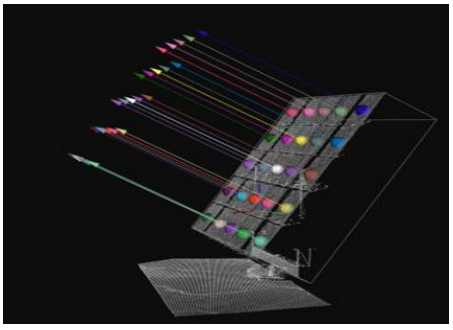

FIGURE 11. Canting angles shown with heliostat scan data.

Comparison of Front Versus Back Surfaces

From the beginning, it was speculated that equivalent results could be obtained by scanning the back of the heliostat. On many of the heliostats observed, the back side has the majority of the facet visible even with the support structure. The facets themselves are composed of a glass plate, with a mirror coating. At NSTTF, their facets are glued to a steel support structure that is then bolted to the heliostat frame. Figure 12-A shows a photo of the back of an NSTTF heliostat. At the Crescent Dunes Solar Energy Project in Tonopah, Nevada, their facets us a different design, and have a support frame fabricated directly onto the back of the mirror, as shown in the back-side photo in figure 12-B. Both of these support structures can be seen in the point scan data, as shown in figure 12-C and figure 12-D respectively.

As seen in the images, a substantial portion of the facet is visible from the back. If this can be isolated, it should be able to be used to estimate the facet and therefore its pointing direction. Unfortunately, the NSTTF back side is itself a reflective surface, and proved to be unusable for facet estimation. However, the Crescent Dunes heliostat back side are painted white and scanned cleanly. The data was filtered to remove the support structure, as shown in figure 13.

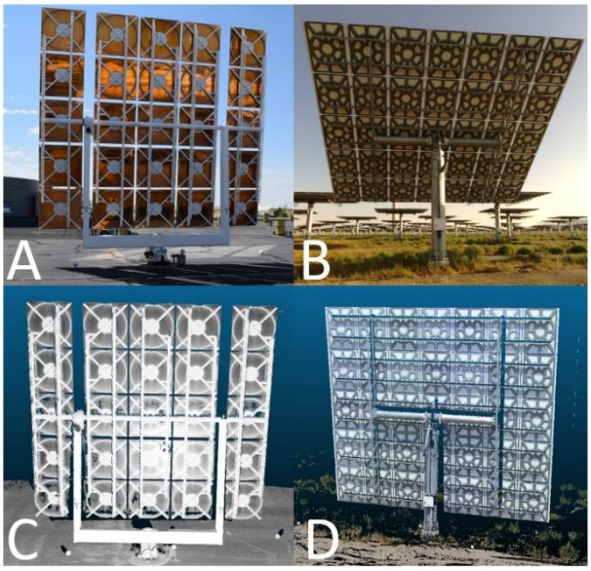

FIGURE 8. A - Back of NSTTF heliostat. B - Back of Crescent Dunes heliostat. C - LiDAR scan of back side, NSTTF. D - LiDAR scan of back side, Crescent Dunes.

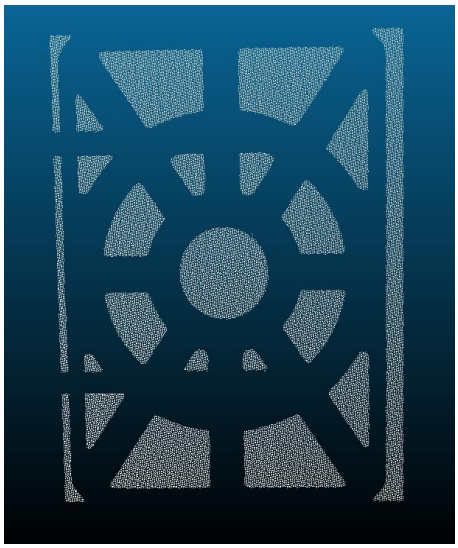

FIGURE 9. The filtered back-side data of a Crescent Dunes facet.

It was presumed the facet normal data for the plane should be the same for the front-side scan and back-side scan. Scans from the front and back for the Crescent Dunes data were registered into a common coordinate frame. This was enabled by placing targets around the base of the heliostat that could be seen by both the front and back scans before the scanning took place. The common targets provided the necessary registration data. The normals were expressed in azimuth and elevation as noted earlier. The comparison of front-to-back results were favorable, with the mean errors for the 35 facets at 0.124 mrad for azimuth and 0.004 mrad for elevation. The standard deviation values were 0.98 mrad azimuth and 0.81 mrad elevation.

REPEATABILITY STUDY

A repeatability study was performed at the NSTTF which acquired more than 230 individual scans of 13 heliostats at 3 different elevation angles. Each heliostat was scanned at 3 or 4 different heliostat elevation angles; 0° (vertical), 25°, 30° and 45°. Multiple scans (between 5 and 9) were taken at each discrete elevation angle. The relative canting angles where then derived for each scan. The standard deviation of the derived azimuth and elevation angle was calculated for each individual facet within that set of scans. The RMS error of the standard deviations was taken for

each heliostat data set, yielding 40 discrete RMS errors in azimuth and elevation. The average RMS error in Azimuth was 0.21 mrad, and the average RMS error of Elevation was 0.20 mrad.

GRAVITATIONAL EFFECTS ON REPEATABILITY

Data collected at three elevations was considered. Deviations were observed when comparing the relative canting angles between the same heliostat at different elevation angles, which is suggested to be the deflection of the mirror facets due to gravity. In [6] the authors performed modelling that showed a maximum displacement of 5.6 mm in the heliostat structure due to gravity. Simulation results from that paper are shown in figure 14. This translates into potential displacements of 2.0 mrad to 2.8 mrad in the canting angles. This implies that the canting angles change significantly with the elevation angle, and that the relatively tight results for RMS error in scans at the same heliostat elevation angle can be expected to change. This is consistent with the result found when considering the average facet RMS data for multiple elevations, which for the 13 heliostats across all elevation angles was 0.49 mrad in facet azimuth and 1.22 mrad in facet elevation.

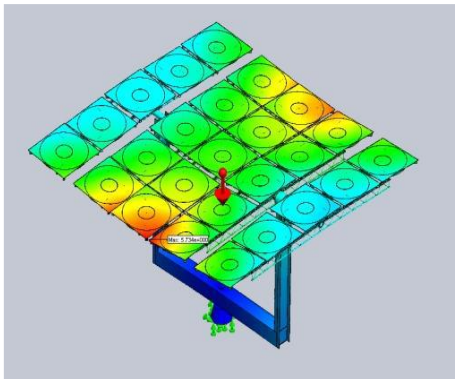

FIGURE 10. Gravity deformed heliostat in horizontal orientation [6]

LIMITS TO CANTING ANGLE ESTIMATIONS

One of the primary goals of this work is to develop a system to measure heliostat canting errors to less than 0.25 mrad accuracy. The canting angle calculations are only as good as the accuracy of the plane fit. As mentioned earlier, it is known that, in fact, the facets do have a slight parabolic shape. Because the parabolic shape is minimal and centered on the facet, it was assumed that a planar fit of all the surface data is an adequate estimate of the facet angle.

Several other factors were examined. The first is the effect of the point density, or number of points on the facet. Simulated LiDAR scans of facets were placed at known positions and angles, relative to the simulated sensor, and point density and range noise were also varied. Comparisons were made between the input angles and calculated angles. Assuming the range noise to be ± 0.002 mm (the declared noise level of the scanner used), a thousand simulations with 2 mm added noise were averaged to find the standard deviation for point counts between 100 and 100,000. Figure 15 shows this data in a chart. The X axis is the number of points on the facet, and the Y axis is the standard deviation of the normal expressed as the azimuth angle. The blue plot are the values calculated. The red plot is the normalized $\frac{1}{\sqrt{(N)}}$ showing the error value does indeed follow the rule of error reduction with increased points to analyze. Past a thousand points (0.048 mrad RMS), these numbers are significantly below the 0.25 mrad target.

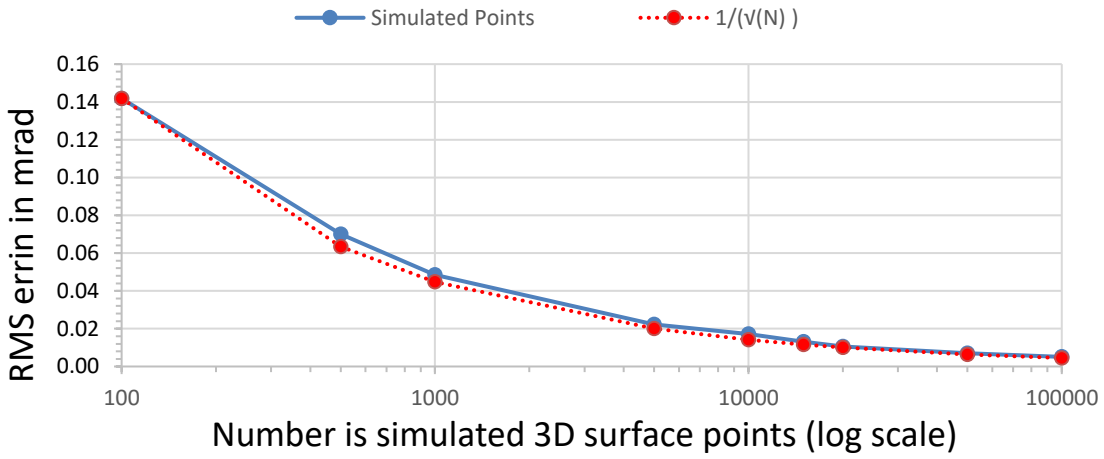

FIGURE 11. Plot of RMS error versus number of scan points on the facet.

A second factor considered here was the effect of the angle of the facet to the scanner. It was supposed the larger the angle, the greater the error. The simulation testing, at 0° (straight-on) to 60° off-axis to the sensor showed no noticeable difference in error, showing similar standard deviation errors as the previous test, well below the target goal. While this is optimistic in terms of how the heliostat can be scanned in the field, it is still assumed large off-angle scanning will have a detrimental effect on accuracy. Most surfaces will have a reduction in laser intensity relative to the incident angle with the scan beam, The lower the intensity, the greater the range error. The position of the scanner relative to the heliostat will have a direct relation to this incident angle. When the scanner is close to the heliostat, this angle to the lower facets versus upper facets can vary significantly. This effect has not yet been verified in the field.

CONCLUSIONS

This project considered the use of processed 3D point-cloud LiDAR scans of heliostats to calculate in-situ measurements of canting angles in the field. It has been shown that LiDAR scanning is possible for valid data collection to measure heliostat facet canting angles, demonstrating this process in over two hundred field scans. The effects of facet soiling on the scanning process has been noted and workable solutions for mirrors that are too clean have been found. The possibility to use either the front or back side of the heliostat for this process has been addressed; however, where possible, the front side is recommended, primarily because it is unencumbered by support structures, and some heliostat designs do not expose the back-side mirror surface. The effects of measurement noise in the calculations of plane fitting accuracy has also been addressed. The entire remote scanning and processing from a laptop computer has been automated, which can complete the entire process in less than 5 minutes per heliostat. Based on the heliostats tested, and the repeatability studies conducted, It is proposed that the 0.25 mrad error accuracy requirements given at the start of this project has been achieved.

FUTURE WORK

It was initially hoped to tackle the tracking error problem by using the position data available in the scan, such as the base of the heliostat, and match it with real GPS locations. The results were never accurate enough in initial attempts. It is assumed this is because the available GPS data of heliostat positioning was itself not accurate enough to reach the desired levels of 0.5 mrad error. This needs further study to see if this, or some other method, can use readily available localization information to accomplish this task.

Since LiDAR scanning does not require external or ambient light this method is also amenable to data collection when the sun is not shining; whether on cloudy days, early morning or evening, or even at night.

Potential for Autonomous Data Collection

It is considered possible to mount the scanner and computer on a mobile platform and automate the heliostat scan process. The mobile platform would drive to a designated spot in front of each heliostat. This is doable with path planning and collision avoidance onboard the mobile platform to avoid driving issues. The platform would then initiate the scan, process the data, and move to the next heliostat. Some coordination with the field operation to place the heliostats in an acceptable position would also be needed. LiDAR scanners have already been deployed on commercial ground and air vehicles. Figure 16 shows a recently available commercial product from FARO Technologies called Trek [7]. This places a FARO scanner, like the one used for this project, mounted on the back of SPOT, a robotic platform from Boston Dynamics.

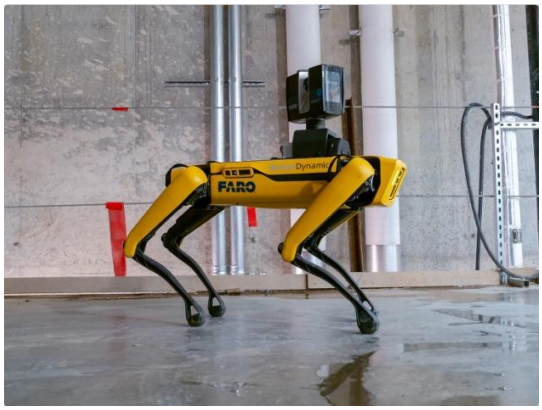

FIGURE 12. FARO Trek; a LiDAR scanner on a mobile platform.[7]

ACKOWLEDGEMENTS

Sandia National Laboratories is a multimission laboratory managed and operated by National Technology & Engineering Solutions of Sandia, LLC, a wholly owned subsidiary of Honeywell International Inc., for the U.S. Department of Energy's National Nuclear Security Administration under contract DE-NA0003525. The authors would like to thank the DOE Solar Energy Technology Office for supporting this research.

REFERENCES

1. E. Sproul, K. Chavez, J. Yellowhair, Heliostat Focusing and Canting Enhancement Technique: An Optical Heliostat Alignment Tool for the National Solar Thermal Test Facility, ES2011-54268, *Proceedings of the ASME 2011 5th International Conference on Energy Sustainability*, Washington, D.C, Aug. 7-10.
2. K. Chavez, E. Sproul, J. Yellowhair, Heliostat Facet Focusing and Characterization using the Heliostat Focusing and Canting Enhancement Technique, *Proceedings of the ASME 2012 6th International Conference on Energy Sustainability*, San Diego, CA, July 23-26.
3. Yellowhair, P. A. Apostolopoulos, D. E. Small, D. Novick, M. Mann, Development of an Aerial System for Heliostat Canting Assessments, *Proceedings of SolarPACES 2020 Online Conference*, Sept. 28 – Oct. 2.
4. Faro Focus Laser Scanners, https://www.faro.com/en/Products/Hardware/Focus-Laser-Scanners
5. Bounding Box Algorithm, https://github.com/GeoDaCenter/geoda/blob/master/libgdiam/README
6. A. C. Moya, C. K. Ho, Modeling and Validation of Heliostat Deformation Due to Static Loading, Proceedings of the ASME 2011 5th International Conference on Energy Sustainability & 9th Fuel Cell Science, Engineering and Technology, August 7-10, 2011, Washington DC, USA
7. Faro Trek 3D Laser Scanning Integration, https://www.faro.com/en/Products/Hardware/Trek-3D-Laser-Scanning-Integration